ELSEVIER

Polymer 40 (1999) 2561–2568

polymer

X-ray studies on the smectic polymorphism of chiral polysiloxanes with a sulfide substituent

Bernard Gallot[a], Giancarlo Galli[b], Antonio Ceccanti[b], Emo Chiellini[b,*]

[a]*Laboratoire des Matériaux Organiques a Propriétes Spécifiques, CNRS, 69390 Vernaison, France*
[b]*Dipartimento di Chimica e Chimica Industriale, Università di Pisa, 56126 Pisa, Italy*

Received 17 March 1998; accepted 8 June 1998

Abstract

A new class of chiral liquid-crystalline polysiloxanes was synthesised, and their thermotropic behaviour and mesophase structure were investigated. The mesogenic side chains consisting of a three-phenyl core were connected to the siloxane polymer backbone by an alkylene spacer segment of varying number *m* of methylene units and of a chiral sulphide substituent. An X-ray diffraction study of powder and fibre specimens permitted to elucidate the structure of the mesophases, which in any case resulted in tilted, monolayer types. Polysiloxanes **P8**, **P10** and **P11** incorporating longer spacers with $m = 8$, 10, and 11, respectively, exhibited a rich variety of smectic mesophases. The smectic I–smectic F–smectic C phase sequence with rising temperature was identified in all three samples by analysis of the wide-angle diffraction. Three-dimensionally ordered structures were also formed at low temperatures. The various low-angle reflections on the smectic layers were used to evaluate the projections of the electron density profiles along the layer normal, and the most physically acceptable profiles were selected from the numerous possibilities for each smectic mesophase.

Keywords: Liquid-crystalline polymers; Polymorphism; Smectic I

1. Introduction

Three-phenyl mesogenic cores, such as **I** or **II**, have recently been incorporated into various liquid-crystalline (LC) polymer architectures; for some latest developments see Refs. [1–6].

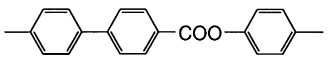

I

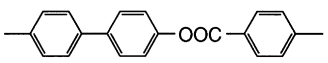

II

In fact, chiral polymers consisting of **I** or **II** in combination with suitable chiral substituents are known to be capable of giving rise to the chiral smectic C phase [3–14], which is of great current interest for many applications including switching devices, electro-optic displays, recording media and nonlinear optical effects [15]. The occurrence of the chiral smectic C and other smectic phases is very sensitive to fine chemical details, and simple reversal of the ester group orientation in **I** and **II** can be expected to form different smectic phases in otherwise identical LC polymers. A diversity of chiral groups was thoroughly investigated for inducing chirality in LC polymers, the most common substituents being chiral alkyloxy groups [3–14]. Chiral sulphide groups have recently been used as the terminal substituents of the mesogenic unit of LC polymers [16–18]. The sulphur atom has indeed a greater size and polarisability than the oxygen atom, which can also substantially affect the thermotropic behaviour of LC molecules. In addition, the functional sulphide –S– group can undergo chemical modifications, including the enantioselective oxidation to the chiral sulfoxide –S*(O)– moiety, for the realisation of unconventional LC structures [17,18].

In this work, the effects of structural variations on the formation of smectic phases, especially the smectic C phase, were investigated in a new class of chiral LC polymers consisting of a three-phenyl mesogenic moiety variously spaced from a siloxane backbone and bearing a

* Corresponding author.

0032-3861/99/$ - see front matter
PII: S0032-3861(98)00459-5

terminal chiral sulphide substituent:

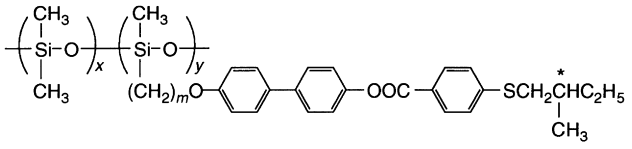

P4, P8, P10, P11 (m = 4, 8, 10, 11; y = 35, x = 0)
O11 (m = 11; y = 4, x = 0)
C11 (m = 11; y = 7, x = 7)

Homopolymers **P4**-**P11**, oligomer **O11**, and copolymer **C11** were investigated, as they were expected to exhibit a rich smectic polymorphism, including ordered and disordered smectic phases. Another objective of the work was to investigate the smectic structures by X-ray diffraction on powder and fibre samples. The intensity of the diffraction signals in the low-angle region was used to derive the electron density profiles along the smectic layer normal, and the most physically acceptable ones, were identified.

2. Experimental

2.1. Materials

The platinum divinyltetramethyldisiloxane complex in xylene solution (3 wt% from Petrarch) was handled under nitrogen and used as received. Siloxane homopolymers **P4–P11**, oligomer **O11**, and copolymer **C11** were synthesised by an hydrosilylation reaction of olefin monomers ($m = 4$, 8, 10, or 11) onto the corresponding methylhydrosiloxane (from Petrarch) homopolymer ($x = 0$, $y \approx 35$), oligomer ($x = 0$, $y \approx 4$), and copolymer ($x \approx 7$, $y \approx 7$), respectively. A typical hydrosilylation reaction is described here for the synthesis of polysiloxane **P11**: A solution of 1.06 g (1.9 mmol) of (+)-(*S*) 4-[4′-(10-undecenyloxy)]biphenyl 4-(2-methyl-1-butylthio)benzoate ($m = 11$), 0.101 g (1.7 mmol Si–H groups) of poly(methylhydrosiloxane) ($x = 0$, $y \approx 35$) and a catalytic amount (0.004 mmol) of platinum divinyltetramethyldisiloxane in 30 ml of anhydrous toluene was heated to 60°C for 3 h under nitrogen atmosphere until the Si–H absorption of 2150 cm^{-1} disappeared. After an additional 8 h reaction, the polymer was precipitated into methanol and then purified by repeated precipitations from chloroform solution into methanol and finally by extraction with diethyl ether (yield 79%). $[\alpha]_D^{25} = +8.4°$ ($CHCl_3$). ^{1}H–NMR ($CDCl_3$) δ_H 8.1 (m, 2 H, aromatic), 7.5 (two m, 4 H, aromatic), 7.4 (m, 2 H, aromatic), 7.1–6.9 (two m, 4 H, aromatic), 4.0 (m, 2 H, CH_2OAr), 3.0 (two m, 2 H, SCH_2), 2.2–0.9 (m, 27 H, aliphatic), 0.3 (m, 2 H, CH_2Si), 0.1 (m, 8.5 H, CH_3Si).

2.2. Physicochemical characterisation

Average molecular weights of the polymers were evaluated by size exclusion chromatography (SEC) using a Perkin–Elmer 2/2 chromatograph equipped with Shodex A802/S and A803/S columns and a Perkin–Elmer LC75 ultraviolet detector with THF elution. Monodisperse polystyrene samples were used for calibration.

Optical polarising microscopy observations of the mesophase textures were carried out on thin films between glass slides without any previous treatment with a Reichert Polyvar microscope equipped with a Mettler FP52 heating stage.

Differential scanning calorimetry (DSC) analysis was carried out with a Mettler TA4000 system using 10 K min^{-1} scanning rate. The transition temperatures were taken as corresponding to the maximum in the enthalpic peaks in the DSC traces of samples that had been annealed by cooling from the isotropic melt. Indium standard samples were used as the reference for enthalpy evaluation from the integrated peak areas. The glass transition temperature was taken at the temperature of half-devitrification.

X-ray diffraction experiments were performed on powder and fibre samples with a pinhole camera with Ni-filtered CuKα beam ($\lambda = 1.54$ Å) at various temperatures between 20 and 250°C ($\pm$ 1°C). Several exposures were taken so as to measure the strongest and the weakest reflections. Intensities I_n of the reflections were measured with a home-made microdensitometer specially designed to analyse X-ray diagrams provided by linear focusing and pinhole cameras. Experimental amplitudes a_n of diffraction of the different orders of reflections on the smectic layers were corrected for the Lorentz-polarisation factor [19] and normalised to that of the strongest one (Table 1).

3. Results and discussion

3.1. Synthesis and thermal properties

LC siloxane homopolymers **P4–P11** ($y \approx 35$; $x = 0$),

Table 1
Amplitudes[a] of the low-angle reflections of different smectic mesophases of the LC polysiloxanes

Amplitude	**P11**			**O11**		**C11**	
	SmI	SmF	SmC	SmF	SmC	SmF	SmC
a_1	1	1	1	1	1	1	1
a_2	0.53	0.47	0.57	0.44	0.47	0.44	0.52
a_3	0.36	0.31	0.26	0.29	0.30		

[a]After normalisation to the amplitude of the strongest reflection.

Table 2
Physicochemical and thermal properties of the LC polysiloxanes

	$[\alpha]_D^{25}$ [a] (deg)	M_n [b] (g mol^{-1})	Phase transitions [c]
P4	+8.1	24 000	SmF 101 (0.7) SmC 149 N (0.5) 185 (0.4) I
P8	+8.1	29 000	CrH 112 (7.5) SmI 129 (≈ 0.3) SmF 183 (≈ 0.2) SmC 199 (2.1) I
P10	+6.7	21 000	CrH 96 (6.1) SmI 110 (≈ 1.4) SmF 185 (≈ 0.2) SmC 201 (3.9) I
P11	+8.4	28 000	g 44 CrH 105 (5.5) SmI 123 (2.3) SmF 206 (0.3) SmC 223 (3.9) I
O11	+6.4	4 000	CrH 106 (7.7) SmF 130 (2.4) SmC 199 (6.2) I
C11	+8.4	34 000	K 107 (13.4) SmF 122 [d] (nd) [d] SmC 189 (9.0) I

[a] Optical rotary power, in chloroform.
[b] By SEC, with polystyrene calibration.
[c] Transition temperatures (in °C) and enthalpies (in kJ mol^{-1}), in parentheses, by DSC; for phases and symbols, see text.
[d] Not detectable by DSC.

oligomer **O11** ($y \approx 4$; $x = 0$), and copolymer **C11** ($y \approx x \approx 7$) were prepared by grafting the corresponding side-chain olefin monomers ($m = 4$, 8, 10, or 11) onto preformed hydrosiloxanes by a polymer analogous hydrosilylation reaction catalysed by a Pt complex, according to a conventional procedure [20]. The synthesis and thermotropic and electro-optic properties of the monomers appear of rather special interest and will be reported elsewhere.

Each LC siloxane sample exhibited a number of mesophases, which therefore occurred in polymorphic sequences below the isotropic melt (I), as summarised in Table 2. All mesophases were identified as smectic by X-ray diffraction, except the highest temperature mesophase of **P4** which was chiral nematic (N). The thermal stability of the mesophase was rather high, the lowest isotropisation temperature (T_i) in the series being observed for **P4** at 185°C. It was difficult to detect the glass transition temperature (T_g), e.g. at 44°C for **P11**, presumably because of a great rigidity of the polymer backbone in the glassy smectic mesophase which remained frozen-in at room temperature. The LC range was broadest for **P11**, being $T_i - T_g = 179$°C. Copolymer **C11** was semicrystalline (see later) and presented a relatively high melting temperature (T_m) at 98°C. Thus, its LC range was the narrowest in the series investigated, being $T_i - T_m = 91$°C.

Visual observations of the birefringent textures at the polarising microscope enabled us to confirm qualitatively the LC behaviour of the polymers. On cooling from the isotropic melt, the mesophase usually nucleated in small batonnets which afterwards coalesced in bigger domains resembling the smectic focal-conics. However, in no cases were specific textures observed which could assist in identifying unequivocally the mesophases and relevant transitions.

3.2. X-ray patterns

In general, the X-ray diagrams of the different phases, except for the nematic phase of **P4**, exhibited in the low-angle region, two or three sharp reflections with Bragg spacings in the ratio 1:2:3 typical of layered structures. For each phase, the thickness d of the layered structures was always much shorter than the length L of the polymer repeating unit, as

Table 3
Lattice parameters [a] of the different phases of the LC polysiloxanes

	P4	**P8**	**P10**	**P11**	**O11**	**C11**
$L \pm 0.5$ Å	31.0	36.0	38.5	40.0	40.0	40.0
Structure	SmF	CrH (or CrK)	CrH (or CrK)	CrH (or CrK)	CrH (or CrK)	K
$d \pm 0.2$ Å	26.0	31.6	34.0	35.2	36.5	38.0
$a \pm 0.1$ Å	5.7	4.8	4.8	4.8	4.8	4.5
$b \pm 0.1$ Å		4.2	4.2	4.2	4.3	3.6
θ/deg	33	29	28	28	24	18
Structure	SmC	SmI	SmI	SmI	SmF	SmF
$d \pm 0.2$ Å	26.0	31.6	33.0	35.2	36.5	38.0
$a \pm 0.1$ Å	4.8	5.7	5.7	5.6	5.5	5.2
θ/deg	33	29	31	28	24	18
Structure		SmF	SmF	SmF	SmC	SmC
$d \pm 0.2$ Å		31.6	34.0	34.5	36.5	36.8
$a \pm 0.1$ Å		5.7	5.6	5.5	4.8	4.5
θ/deg		29	28	30	24	23
Structure		SmC	SmC	SmC		
$d \pm 0.2$ Å		33.3	36.0	36.8		
$a \pm 0.1$ Å		4.8	4.8	4.9		
θ/deg		22	21	23		

[a] For phases and symbols, see text.

measured on the CPK stereomodels (Table 3). In low molar mass liquid crystals the spacing d for various orthogonal smectic phases, like the A, B, or E phases, can be shorter than the calculated L, because of the conformational freedom of the molecules in the mesophase and their thermal displacement along the director [21], which results in a decrease of the periodicity d. However, in LC polymers, in which the mesogenic side chains are connected to the polymer backbone by means of a spacer segment, their overall motion is more restricted with respect to the rather freely moving molecules of the low molar mass counterparts. In the present polymers, incompatibility between the siloxane polymer chain and the mesogenic side chains could impose additional constraints on their mobility, thereby reducing the thermal displacement along the director of the smectic mesophases. Thus, the difference between d and L may be accounted for by a tilt of the side chains with respect to the layer normal, and the various phases were of the tilted monolayer types ($d < L$). The tilted character of the structures was confirmed by the X-ray diagrams of oriented fibres of copolymer **C11**, in which the Bragg layer reflections appeared on the equator and the wide-angle reflection was split into four symmetrical arcs (Fig. 1). Therefore, the layers were oriented parallel to the fibre axis and the molecules were tilted to the layer normal, a tilt angle, θ, of 32° being measured at room temperature.

The X-ray patterns differed by the aspect of the wide-angle region, which allowed the division of the different phases into three groups. The first family exhibited, in the wide-angle domain, three sharp rings (Figs 2 and 3), that could be provisionally indexed on a rectangular lattice of parameters a and b (Table 3). Accordingly, the structure could be either crystalline (K) or 3-D ordered smectic, H or K. The latter are in fact soft crystalline structures and are conventionally referred to as crystal H (CrH) or K (CrK).

The second family exhibited, in the wide-angle region, one sharp reflection characteristic of a pseudo-hexagonal array of the hexatic smectic F (SmF) or I (SmI) phases (Figs 4 and 5), with the side of the hexagon being $a \approx 5.6 \pm 0.1$ Å (Table 3). The SmF and SmI phases are both tilted, but for the SmF phase the tilt of the long molecular axis is towards a side of the hexagon, while for the SmI phase the tilt is towards an apex of the hexagon (Fig. 6). In neither case is there a significant distortion from the hexagonal packing and for both phases the unit cell is C-centred monoclinic [22]. However, the in-plane correlation length of the SmI phase is by far greater, up to four times, than in the SmF phase, and therefore in the SmI phase the wide-angle ring is sharper than in the SmF phase [22,23].

The third family exhibited, in the wide-angle domain, a

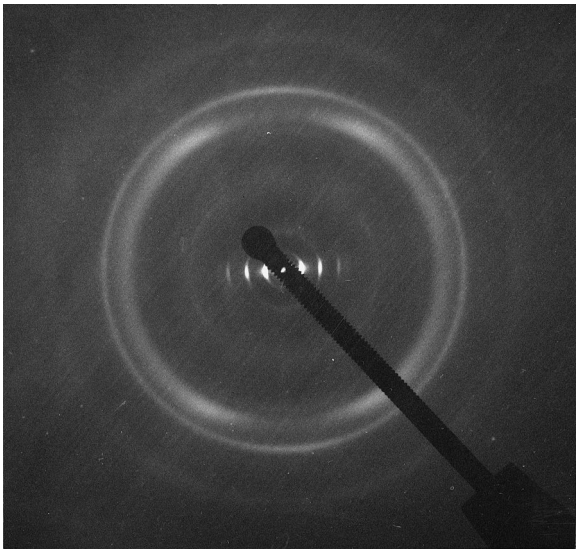

Fig. 1. Fibre X-ray diagram of the crystalline phase of copolymer **C11** at 25°C (vertical fibre axis).

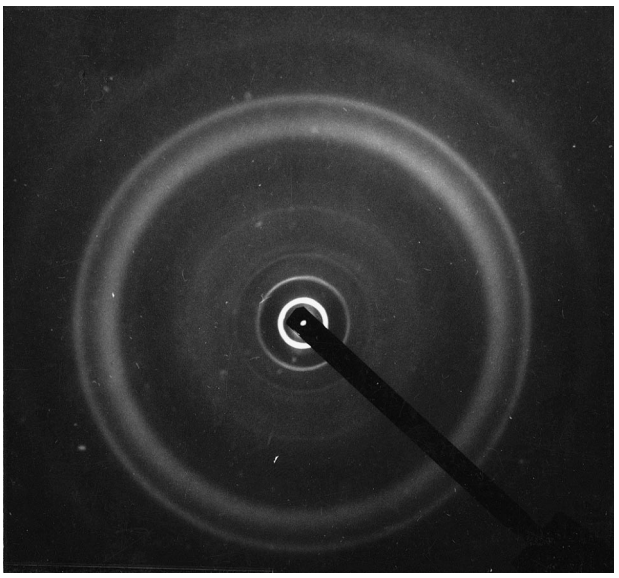

Fig. 2. Powder X-ray diagram of the crystalline phase of copolymer **C11** at 21°C.

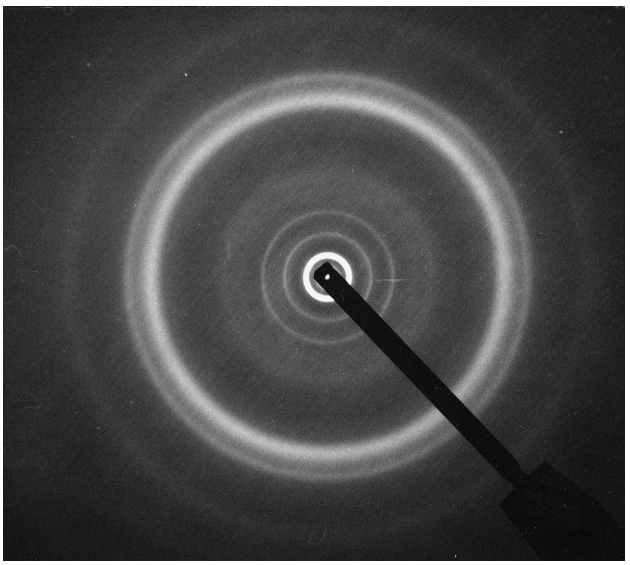

Fig. 3. Powder X-ray diagram of the CrH (or CrK) phase of polymer **P11** at 25°C.

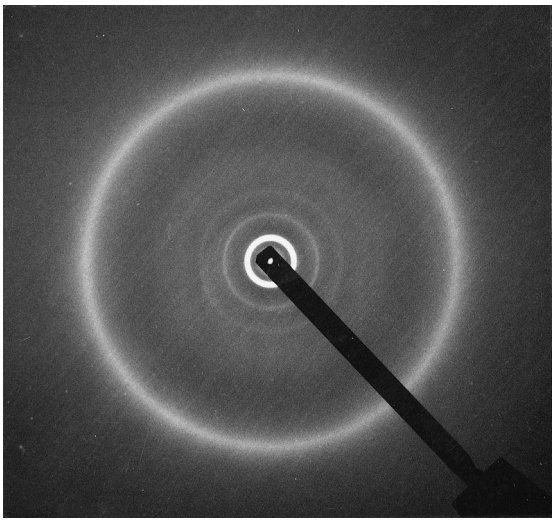

Fig. 4. Powder X-ray diagram of the SmI phase of polymer **P11** at 130°C.

very diffuse band (Figs 7 and 8), intermolecular distance $a \approx 4.8 \pm 0.1$ Å (Table 3), because of the loss of the in-plane correlations between the side-chain mesogens. Consequently the structure was of the smectic C (SmC) type.

3.3. Thermotropic behaviour

Each homopolymer **P8**, **P10** and **P11**, incorporating long spacers, exhibited four phases as a function of temperature. Homopolymer **P4**, oligomer **O11** and copolymer **C11** each presented three phases. In the 3-D ordered, low-temperature phase of **P8**, **P10**, **P11** and **O11**, the surface available per side chain was found to be rather large, that is slightly greater than 20 $Å^2$ (Table 3). This was an argument in favour of the presence of a smectic-like structure such as the CrH (or CrK). However, the surface available for a side chain in the 3-D structure of **C11** was much smaller (16 $Å^2$), which pointed to the occurrence of a crystalline structure in this sample.

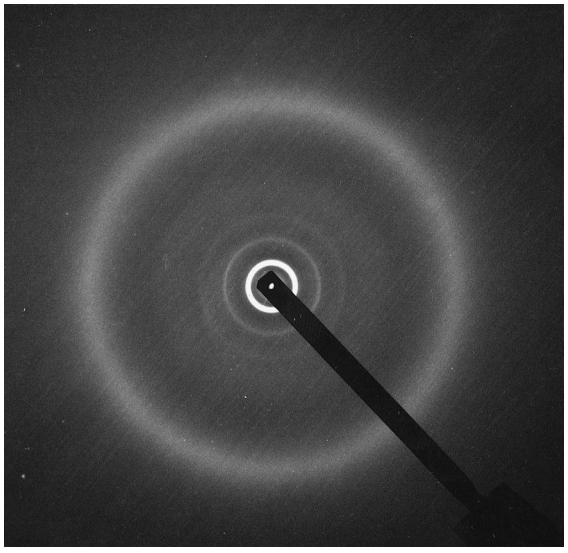

Fig. 5. Powder X-ray diagram of the SmF phase of polymer **P11** at 150°C.

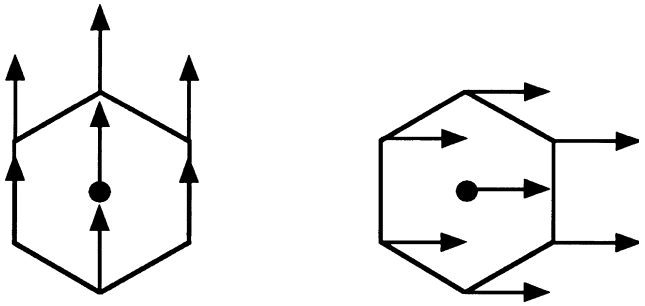

Fig. 6. Schematic representation of the hexagonal packing in the SmI (left) and SmF (right) phases (arrows show the direction of the tilted mesogens).

The nature of the other high-temperature smectic phases was elucidated by a study of the variation in the width of the wide-angle ring with temperature, as is illustrated in Fig. 9 for **P11**. On increasing temperature, the full width at half maximum (FWHM) of the wide-angle diffraction increased significantly in successive steps reflecting the diminished correlation within the smectic layers in passing from one smectic phase to another. This permitted the location of the SmI–SmF–SmC phase sequence with *increasing* temperature. This sequence appears to be at variance with the behaviour of polymorphic low-molar-mass smectics forming both SmI and SmF phases [22,24,25], for which the SmI phase is usually stable at higher temperature and the SmI–SmF transition occurs with decreasing temperature, for example in the standard sample TBDA [25]. Nevertheless, the type of order in SmI and its relationship to SmF both appear to be anomalous in low-molar-mass smectics [22]. In the present polymers, the connection of the side-chain mesogens to the polymer backbone via a spacer could enforce different local organisations of the mesogens and prevent the formation of a more ordered mesophase at higher temperature, producing the more thermodynamically favourable SmI–SmF–SmC phase sequence. Other

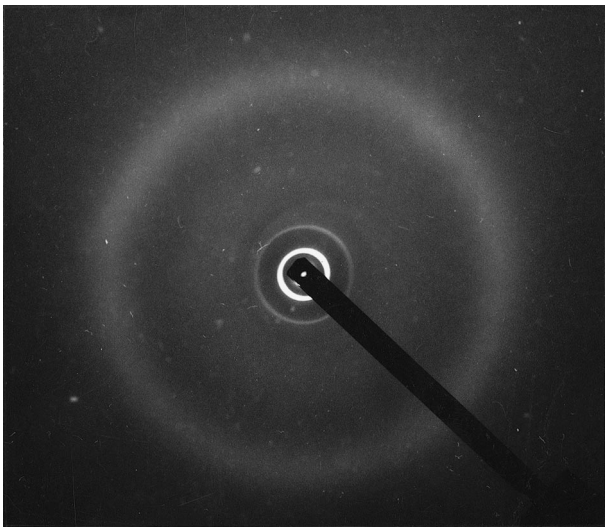

Fig. 7. Powder X-ray diagram of the SmC phase of copolymer **C11** at 165°C.

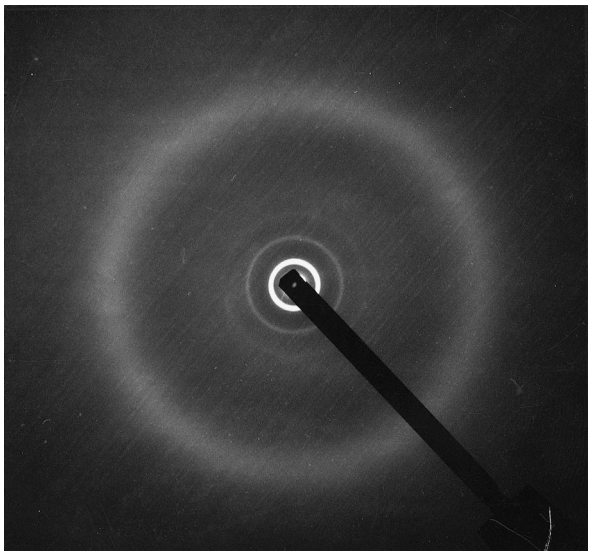

Fig. 8. Powder X-ray diagram of the SmC phase of oligomer **O11** at 170°C.

hexagonal structures are known to occur in liquid crystals in which, however, the smectic layers are also very well correlated and give rise to a 3-D structure, like the crystal G (CrG) or J (CrJ) structures [26,27]. Some of these highly ordered structures have recently been described for LC main-chain polymers [28]. The CrG and CrJ in fact derive from the SmF and SmI, respectively, by development of positional long-range order within and between the layers, while retaining the tilt direction of the molecules. Their X-ray powder diagrams are typical of 3-D structures and normally consist of several wide-angle diffraction rings [21]. This observation is not consistent with our experimental findings and lends further support to the existence of a hexatic smectic, not a crystal smectic below the SmF in **P8**, **P10** and **P11**.

The low-temperature mesophase of **P4** was recognised as SmF in consideration of the relative broadness of its wide-angle reflection [29] as compared to that of the SmF and SmI of **P8**, **P10** and **P11**. Similar arguments applied to **O11** and **C11**. The SmI phase, therefore, vanished in these samples because of a smaller tendency to form smectic phases. This was more evident for **P4**, which in fact gave rise to an N phase at high temperature above the SmC.

Within the range of existence of each layered phase, either crystalline or smectic, the layer spacing d was not affected by temperature, as shown in Fig. 10 for the polysiloxanes. It should be noted that polymers **P8**, **P10** and **P11** had very similar tilt angles within the SmI, SmF and SmC mesophases (Table 3). However, the trends of d, and therefore θ, with temperature were rather different for the three polymers. For example, d increased appreciably at the SmI–SmF transition for **P10**, whereas it decreased at the same transition for **P11** and remained unaffected for **P8**. A rather substantial decrease in θ was detected at the onset of the SmC for each of these three polymers. Notably, θ was constant throughout all the smectic range of **P4** and still as large as 33° at its SmC–N transition. Thus, in the homologous series of polysiloxanes, minor details of the repeating unit structure significantly influenced the fine organisation of the various smectic phases. The measured d for **C11** containing 50% non-mesogenic dimethylsiloxane units was much longer than for **P11** and **O11** especially at low temperature. This lengthening was the result of a microphase separation between the mesogenic side chains and the amorphous siloxane backbone [30] (see Fig. 7), and consequently a smaller apparent θ was evaluated for **C11**.

In a previous work [31] it had been shown that a polysiloxane containing the same spaced side-chain mesogens and the chiral 2-methylbutoxy tail formed various smectic phases, including the C and A phases along with another unidentified low-temperature smectic:

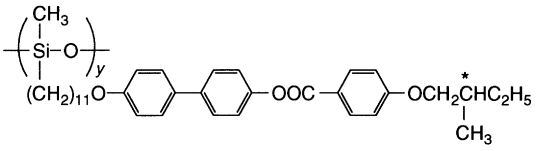

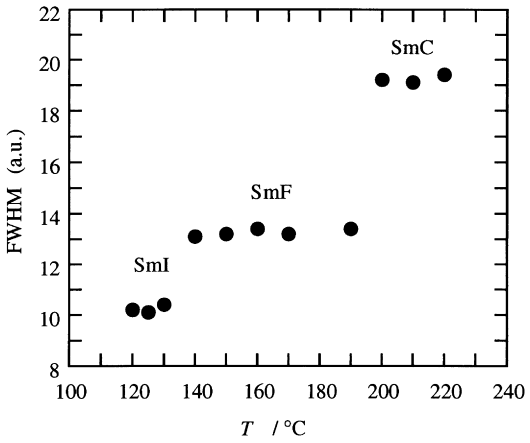

Fig. 9. Full width at half maximum (FWHM) of the wide-angle reflection as a function of temperature for polymer **P11.**

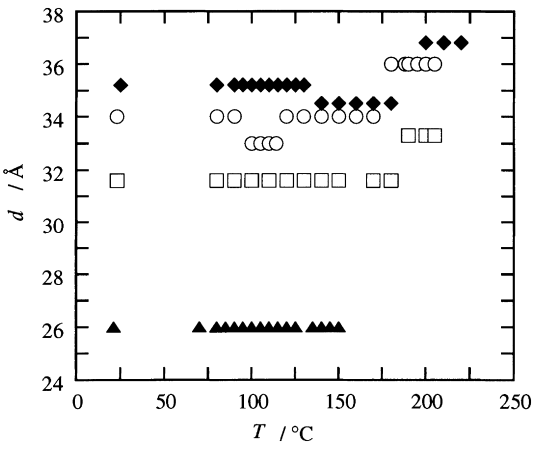

Fig. 10. Variation of the layer spacing d as a function of temperature for polymers **P4** (▲), **P8** (□), **P10** (○), and **P11** (◆).

That sample ($M_n = 27\,400$ g mol^{-1}), however, presented a thermotropic behaviour of a lesser stability, $T_i = 131$°C, extending over a much narrower temperature range, $T_i - T_g = 97$°C, than corresponding **P11**. The liquid crystalline behaviour was preserved in copolysiloxanes incorporating substantial contents of non-mesogenic units [31]. Our findings suggest that simple replacement of the -O- group by the -S- group helped to stabilise the mesophase and enriched its smectic polymorphism.

3.4. Electron density profiles

In order to obtain more information on the organisation of the molecules in the smectic structures, the intensity of the different orders of reflections on the smectic layers of the X-ray diagrams was measured and the corresponding electron density profiles along the normal z to the layers derived.

Taking into account the chemical structure of the molecules, and the fact that only the fluctuations around the average electron density ρ_0, were measured, $\rho(z)$ was given by [32]

$$\rho(z) = \Sigma a_n \cos(n2\pi z/d)$$

As experimentally the intensity I_n of the reflections was measured, the sign of the structure factors a_n was lost, and for n reflections 2^n electron density profiles $\rho(z)$ were obtained [33]. As the X-ray diagrams exhibited three (or two) orders of diffraction for the smectic phases, eight (or four) electron density profiles were deduced. In order to choose the most acceptable $\rho(z)$, the electron densities of the different parts of the repeating unit of the polymers were calculated by dividing their numbers of electrons by their lengths measured on the CPK models. They were found to be 9.5 e Å^{-1} for the mesogenic core, 6.4 e Å^{-1} for the spacer, 8.8 e Å^{-1} for the sulphide tail, and 7.8 e Å^{-1} for the backbone considering it as confined in the smectic planes.

To illustrate this procedure, take the example of the SmC phase of **O11**. In Fig. 11 only the four electron density profiles that exhibited a central maximum at the position of the mesogens are depicted, the other four symmetrical profiles being discarded as physically unattainable. Profiles *a* and *d* were rejected because they showed minima for the siloxane main chains and secondary maxima for the aliphatic spacers. Profile *c* was also eliminated because it exhibited a not pronounced maximum for the mesogens and very high values of the electron density for the spacers. Profile *b*, corresponding to the ρ_{-++} combination, was chosen as the most physically acceptable one because it presented a central prominent maximum for the mesogenic cores, surrounded by minima for the spacers and secondary maxima for the main chains as one should expect to observe for monolayer smectic phases.

The same simple structural considerations also lead to the choice of the ρ_{-++} electron density profile for the other smectic phase of **O11** and for the three smectic phases of **P11** (Fig. 12). The ρ_{-+} profile was chosen for the two

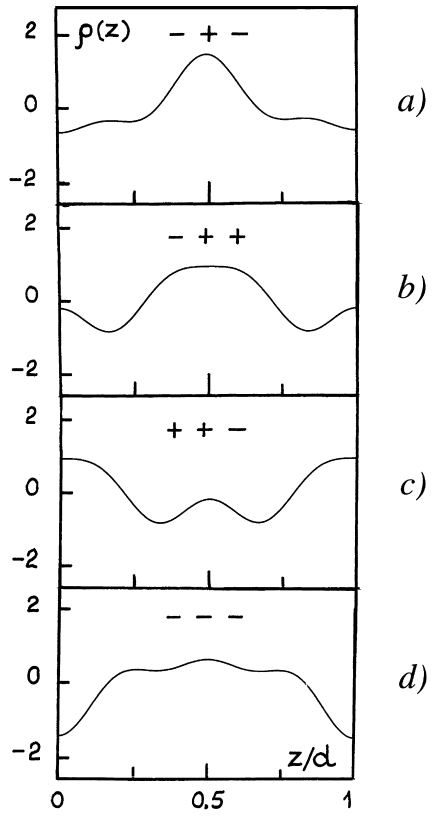

Fig. 11. Electron density profiles $\rho(z)$ for different sign combinations of a_n for the SmC phase of oligomer **O11**: (a) ρ_{-+-}; (b) ρ_{-++}; (c) ρ_{++-}; (d) ρ_{---}.

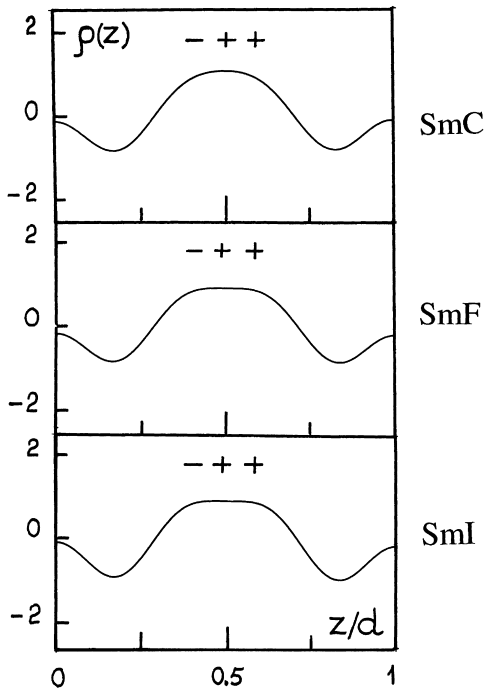

Fig. 12. Electron density profiles ρ_{-++} for the SmI, SmF and SmC phases of polymer **P11**.

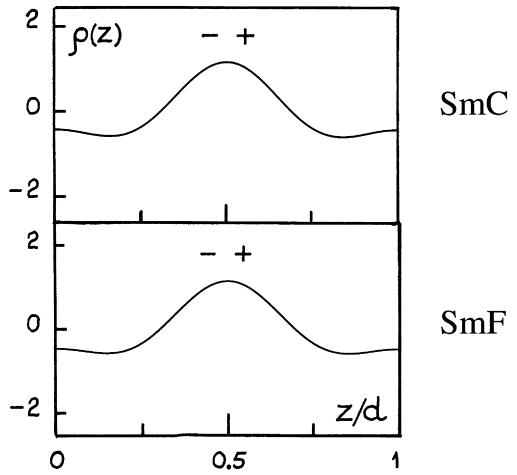

Fig. 13. Electron density profiles ρ_{-+} for the SmF and SmC phases of copolymer **C11**.

smectic phases of **C11** which both presented two low-angle reflections (Fig. 13).

4. Concluding remarks

All the siloxanes studied exhibited a rich polymorphism, the richer one being observed for polysiloxanes with long spacers ($m = 8$, 10 or 11) which formed four tilted, monolayer smectic phases as a function of temperature. For these samples, polymorphism included one 3-D ordered, two hexatic hexagonal and one disordered smectic structures. This is in keeping with incorporation in the repeating unit of three-phenyl mesogenic cores spaced from the polymer main chain by a long alkylene segment. Characterisation of the SmF and SmI phases in polymers is typically very difficult, and, to the best of our knowledge, the SmI–SmF–SmC sequence has never been disclosed before. The propensity to form smectic phases appeared to be enhanced by using the terminal sulphide substituent, which in addition provided chirality and optical activity to the molecular structure. By analogy to low-molar-mass chiral smectics [34], one could assume that in polymers the molecular tilts also lie in the same direction in any domain, and that the tilt directions will consistently be turned on moving from one layer to the next and will thereby form a macroscopic helical assembly with one prevailing screw sense even in the SmI and SmF phases, as is well known for the SmC phase.

Acknowledgement

Work performed with financial support from the Italian National Research Council, Comitato Tecnologico and Progetti Bilaterali.

References

[1] Hempenius MA, Lammertink RG, Vancso GJ. Macromolecules 1997;30:266.
[2] Akiyama E, Matsui N, Nagase Y. Liq Cryst 1997;23:425.
[3] Mery S, Lötzsch D, Heppke G, Shashidhar R. Liq Cryst 1997;23:629.
[4] Hsu C-S, Tsai C-H. Liq Cryst 1997;22:669.
[5] Buxton IP, Hall AW, Lacey D. Macromol Chem Phys 1997;198:2307.
[6] Cooray NF, Fujimoto H, Kakimoto M, Imai Y. Macromolecules 1997;30:3169.
[7] Kapitza H, Zentel R, Twieg RJ, Nguyen C, Vallerien SU, Kremer F, Willson CG. Adv Mater 1990;2:539.
[8] Kühnpast K, Springer J, Scherowsky G, Giesselmann F, Zugenmaier P. Liq Cryst 1993;14:861.
[9] Schberowsky G, Fichna U, Wolff D. Liq Cryst 1996;20:673.
[10] Skarp K, Andersson G, Gouda F, Lagerwall ST, Poths H, Zentel R. Polym Adv Technol 1992;3:241.
[11] Nishiyama I, Goodby JW. J Mater Chem 1993;3:169.
[12] Naciri J, Pfeiffer S, Shashidhar R. Liq Cryst 1991;10:585.
[13] Chien L-C, Shenouda IG, Saupe A, Jakli A. Liq Cryst 1993;15:497.
[14] Shenouda IG, Chien L-C. Macromolecules 1993;26:5020.
[15] Goodby JW, Blinc R, Clark NA, Lagerwall ST, Osipov MA, Pikin SA, Sakurai T, Yoshino K, Zeks B, editors. Ferroelectric liquid crystals. Amsterdam: Gordon and Breach, 1991.
[16] Laus M, Angeloni AS, Galli G, Chiellini E, Francescangeli O, Yang B. Polymer 1995;36:1261.
[17] Chiellini E, Galli G, Laus M, Angeloni AS, Melone S, Francescangeli O. Mol Cryst Liq Cryst 1995;266:189.
[18] Angeloni AS, Laus M, Caretti D, Chiellini E, Galli G. Chirality 1991;3:307.
[19] Davidson P, Levelut AM, Achard MF, Hardouin F. Liq Cryst 1989;4:561.
[20] Chiellini E, Galli G, Dossi E, Cioni F. Macromolecules 1993;26:849.
[21] Doucet J. In: Luckhurst GR, Gray G, editors. The molecular physics of liquid crystals. London: Academic Press, 1979:317.
[22] Gane PAC, Leadbetter AJ, Benattar JJ, Moussa F, Lambert M. Phys Rev A 1981;24:2694.
[23] Benettar JJ, Moussa F, Lambert M. J Phys (Paris), Lett 1981;42:L67.
[24] Gierlotka S, Przedmojski J, Pura B. Liq Cryst 1988;11:1535.
[25] Gray GW, Goodby JW. Smectic liquid crystals. Glasgow: Leonard Hill, 1984.
[26] Gane PAC, Leadbetter AJ, Wrighton PW, Goodby JW, Gray GW. Mol Cryst Liq Cryst 1983;100:67.
[27] Benattar JJ, Doucet J, Lambert M, Levelut AM. Phys Rev A 1979;20:2505.
[28] Tabrizian M, Bunel C, Vairon J-P, Friedrich C, Noël C. Makromol Chem 1993;194:891.
[29] Ho R-M, Yoon Y, Leland M, Cheng SZD, Percec V, Chu P. Macromolecules 1997;30:3349.
[30] Diele S, Ölsner S, Kuschel F, Hisgen B, Ringsdorf H. Mol Cryst Liq Cryst 1988;155:399.
[31] Wischerhoff E, Zentel R, Redmond L, Mondain-Monvail O, Coles H. Macromol Chem Phys 1994;195:1593.
[32] Gudkov VA. Sov Phys Crystallog 1984;29:316.
[33] Davidson P, Levelut AM, Achard MF, Hardouin F. Liq Cryst 1989;4:561.
[34] Goodby JW. J Mater Chem 1991;1:307.